J. M. Austin, F. Pintgen, and J. E. Shepherd. Reaction zones in highly unstable detonations. In Proceedings of the 30th Combustion Institute, pages 1849–1857, 2005. doi 10.1016/j.proci.2004.08.157.

Reaction Zones in Highly Unstable Detonations

J. M. Austin, F. Pintgen, and J. E. Shepherd

Department of Aerospace Engineering, University of Illinois at Urbana-Champaign, Urbana, IL USA
Graduate Aeronautical Laboratories, California Institute of Technology, Pasadena, CA USA

Abstract

Experimental images of detonation fronts are made for several fuel-oxidizer mixtures, including hydrocarbon-air systems. Schlieren and planar laser induced fluorescence techniques are used to image both the shock configurations and the OH reaction front structure in a single experiment. The experiments are carried out in a narrow rectangular channel. The degree of instability of detonation fronts in different mixtures is evaluated by comparing calculated mixture parameters with the longitudinal neutral stability curve. The images reveal that the structure of the front increases dramatically in complexity as the the mixture parameters move away from the neutral stability curve into the unstable region. Of the mixtures studied, nitrogen-diluted hydrocarbon mixtures are predicted to be the most unstable and these show the greatest degree of wrinkling in the shock and OH fronts, with distortion occurring over a wide range of spatial scales. In the most unstable cases, separation of the shock and OH front occurs and localized explosions in these regions are observed in a high-speed schlieren movie. This is in dramatic contrast to the weakly unstable waves which have smooth reaction fronts and quasi-steady reaction zones with no evidence of localized explosions. A key feature of highly unstable waves is very fine scale wrinkling of the OH and shock fronts which is absent in the low-activation energy cases. This may be due to the superposition of cellular structures with a wide range of cell sizes. In contrast to soot foils, images of the OH front have a more stochastic appearance and organized cellular structure is not as apparent.

Keywords: Detonation, unstable, planar laser induced fluorescence, cellular structure

1. Introduction

Gaseous detonations propagating close to the Chapman-Jouguet velocity all have unstable fronts and there is a large body of work [1–5] documenting the common features of oscillations in the main shock strength, weak shocks moving transversely to the main front, and the quasi-periodic or cellular nature of the disturbances. These features are particularly prominent in mixtures with large amounts of monatomic gas dilution, which make them appealing for numerical or experimental study. In our laboratory, we have recently carried out studies [6–9] using Planar Laser Induced Fluorescence (PLIF) to directly visualize a chemical species (OH) within the reaction zone. We have identified distinctive features of the OH reaction fronts in mixtures with regular cellular systems and shown that they are characterized by smooth OH fronts, with "keystones" of high or low OH concentration located between the trans-

verse waves, and a single characteristic spacing for the transverse waves.

From the very earliest investigations of detonation front structure, it has been clear that there is a bewildering range of behavior depending on the chemical makeup of the mixture being studied [10–13]. These studies have shown that the dynamic response of detonation fronts is dependent on the regularity of the cellular structure. For example, for a given detonation length scale and facility dimension, a mixture with irregular structure may successfully transition through an area change while a mixture with regular structure may fail. In contrast to the sedate instability and regular fronts of mixtures diluted with large amounts of argon, hydrocarbon-air mixtures, which are of greater practical interest, exhibit very unstable and irregular fronts. A key issue is how these instabilities may affect the fundamental combustion mechanism behind the front.

The present paper extends our previous work in two ways: 1) use of a narrow channel in order to reduce the integrating effect of the schlieren images and simplify the interpretation of the corresponding PLIF images, 2) examination of mixtures over a wide range of stability parameters corresponding to a reduced activation energy between 5 and 13. This included mixtures considered by previous researchers to have highly irregular cellular structure. In selecting these mixtures, we have used as a figure of merit for instability the distance from the neutral curve for longitudinal instability in reduced activation energy–Mach number coordinates.

2. Detonation Front Instability

Traditionally, the degree of detonation front instability has been classified by the regularity of the cellular structure as determined from soot foils by visual inspection [14, 15] and image analyses [16]. As an alternative, we use instead the distance from the longitudinal neutral stability boundary in reduced activation energy versus Mach number coordinates as a figure of merit to quantify the degree of instability. For the mixtures considered in this study, the activation energy is the dominant parameter. This choice is motivated by experimental observations [17] and the key role of the activation energy in determining the growth rate of small disturbances in one [18, 19] and two-dimensional [20] treatments of detonation front linear stability.

In the context of a single-step irreversible reaction rate, detonation waves are stable if the activation energy E_a is less than a critical value, which depends on the ratio of specific heats γ, chemical energy content $Q/RT_\circ$ of the mixture, and overdrive factor $f = (U/U_{CJ})^2$. Eckett [21] showed that the one-dimensional neutral stability curve for $f = 1$ is independent of γ if expressed in terms of the reduced activation energy $\theta = E_a/RT_{vN}$, where T_{vN} is the temperature at the von Neumann state, and the CJ Mach number M_{CJ}. In Fig. 1, we show the neutral stability curve of Lee and Stewart [18] in these coordinates together with the parameters for the mixtures considered in the present study. The CJ Mach number for each mixture is calculated [22] using realistic thermochemical properties and the effective activation energy is computed using a detailed chemical reaction mechanism as described in [23].

The mixtures shown in Fig. 1 all have similar M_{CJ} and reduced activation energies ranging from values of $\theta \sim 5$ for highly Ar-diluted mixtures up to $\theta \sim 13$ for the hydrocarbon-air mixtures. As shown in previous soot foil studies, the mixtures closest to the neutral curve show the greatest cellular regularity and those farthest from the neutral stability curve show the least regularity.

3. Experimental Setup

A detonation tube in the form of a narrow channel was built for this study [9]. This design has the advantage of simplifying the flow field by reducing or eliminating entirely the transverse waves propagating in the direction of the smaller dimension. Previous work by other researchers has shown that this arrangement results in some differences in the detonation structure from that observed in a rectangular or circular channel. In particular, Strehlow and Crooker [24] report that the track angle and the calculated transverse wave strength are increased. On the other hand, it is much more straightforward to interpret the schlieren images in a narrow channel than in a square cross section tube. In addition, chemiluminescence is reduced, so that PLIF imaging technique could be used in hydrocarbon detonations. Parameters for representative mixtures considered in this study are given in Table 1 and shown in Fig. 1.

The narrow channel has a 152×18 mm cross section and is 4.2 m long with 150 mm diameter windows. An initiator capable of producing a planar detonation wave from the merging of several wavefronts [25] was used to minimize the initiation transient. The initiator was filled with an acetylene-oxygen mixture which was ignited using a spark plug. Pressure transducers monitored the planarity of the detonation front at the exit plane of the initiator. In addition, four pressure transducers were mounted along the channel to measure detonation pressure and time-of-arrival. From these data, velocity deficits relative to the CJ velocity could be obtained. Ruby laser schlieren [26] and PLIF images of the OH radical [6, 8] were obtained within 800 ns of each other. The two images were then superimposed by postprocessing [6]. Multiple shadowgraph images per experiment were made using a Beckman and Whitley model 189 framing camera [27]. A sequence of 25 images are acquired on Kodak TMAX 400 black and white 35 mm film. The time between images is 832 ns with a 152 ns exposure time. A linear xenon flashlamp excited by a 100 J discharge 50 μs in duration was collimated and used as the light source. Cellular struc-

ture records were obtained using sooted metal sheets mounted on the side wall of the channel at the window location.

Velocity data were taken to gauge if a detonation was in steady-state. In weakly unstable detonation, velocity deficits up to 8% are observed; these increase with increasing argon dilution. As reported by Moen et al. [11], away from propagation limits, the maximum velocity deficits in N_2-diluted H_2-O_2 and hydrocarbon mixtures are less than in the Ar-diluted mixtures. In highly unstable detonations, such as in mixtures of C_3H_8-$5O_2$-$9N_2$, velocity deficits of less than 3% are observed.

4. Weakly Unstable Detonation

Weakly unstable detonations occur in mixtures with stability parameters ($\theta \sim 5$, M_{CJ} 4-6) close to the longitudinal neutral stability curve, see Fig. 1. In particular, this category includes detonations in $2H_2$-O_2 with more than about 50% Ar dilution; these mixtures are well-known [14] to have very regular soot foil patterns.

Images of a detonation in the narrow channel for a weakly unstable detonation in a similar mixture to that studied by Pintgen et al. [6, 8] are shown in Fig. 2. The cell width for this mixture is on the order of 25-35 mm and the separation between the leading shock and OH front can be up to 5 mm depending on the location within the cell. We see features in the schlieren image that are very similar to those observed by previous researchers [1–5]. Triple point configurations in general appear to be of the weak type, irrespective of the location in the cell cycle. The keystone features seen in our previous study [8] are also apparent in Fig. 2b. From the overlay image in Fig. 2 (c), it can now be quite clearly seen that the shear layer originating at the intersection of the main front and transverse wave separates reacted and unreacted gas, forming the boundary of the keystone.

Although the channel is narrow, an instability is excited in the smaller dimension, resulting in a three-dimensional structure. Schlieren images, Fig. 2(c), show two distinct leading features rather than a single leading shock front that would be expected if there were no transverse waves propagating in the smaller dimension. This can be explained by the presence of one or more transverse waves propagating transverse to the light sheet plane. Evidence for this is also seen in the PLIF images, Fig. 2(b), as coherent vertical bands of high OH fluorescence, which can be explained [6] in terms of the intersection of the light sheet with the disturbances of the reaction zone created by the transverse waves propagating perpendicular to the light sheet.

5. Moderately Unstable Detonation

N_2-diluted $2H_2$-O_2 mixtures with $\theta \sim 7$ may be classified as moderately unstable. These mixtures have soot foil patterns that are less regular [9] than those of the weakly unstable mixtures. A sample image of a moderately unstable detonation front is shown in Fig. 3. The main cellular structure has a width of about 25 mm on the soot foils; inspection of the PLIF and schlieren images shows characteristic features separated by 11-13 mm. A secondary system of smaller, random transverse waves is visible on the soot foils with a characteristic width of about 5 mm. These secondary waves, unlike those observed for higher activation energy, are observed throughout the cell rather than being concentrated at the apex. A portion of the front close to the interaction of two triple points is captured in Fig. 3b and c. The PLIF image shows a keystone region of low OH fluorescence that occurs at the end of the cell cycle. An incident wave and several unstable shear layers may be seen in the schlieren image. A portion of the shear layer separates reacted and unreacted gas at the keystone boundary. Alternating layers of high and low OH fluorescence parallel to the main front are visible on the PLIF images. Similar images were observed [7] in a square channel with clear visualizations of the vortex structures characteristic of Kelvin-Helmholtz instability on the shear layers.

5.1. "Unreacted" Pockets

In detonations propagating in the narrow channel, isolated regions of low OH fluorescence are observed at a distance on the order of a cell width downstream of the leading front. Figure 4 shows two isolated low OH fluorescence signal regions downstream of a newly formed Mach stem. These regions appear in cross section to be less than 1 mm wide and 2-4 mm high, located about 7-10 mm behind the main shock front. It is important to note, however, that the detonation in this experiment was traveling with a gradually decaying wave speed and a velocity deficit of 6.5% was measured at the window location, indicating the wave may be failing. Regions of low fluorescence intensity are difficult to observe this far downstream of the shock in hydrocarbon mixtures since the fluorescence intensity decreases more rapidly with increasing downstream distance in hydrocarbon mixtures than in the H_2-O_2 mixtures. The mixture in Fig. 4 had a higher concentration of N_2 than that of Fig. 3 and the cell width was slightly larger, about 36 mm. A similar set of random secondary transverse waves was observed on the soot foils.

6. Highly Unstable Detonation

Schlieren and OH fluorescence images of highly unstable detonation fronts in the narrow channel are shown in Figs. 5 and 6. These fronts contrast markedly with weakly unstable fronts. The lead shock is very irregular and structures over a broader range of scales are apparent. On the soot foils corresponding to Fig. 5, the largest cell widths are 80 mm and smallest substructure cells appear to be 1-2 mm; for Fig. 6, the largest cells are about 60 mm in width and the smallest secondary cells are also 1-2 mm in width.

We observe fine scale (1-2 mm) substructure on soot foils for all N_2O and hydrocarbon mixtures we studied. Substructure has been previously reported in several specific mixtures [14, 15, 28] and in numerical studies [29]. The "keystone" features are not as distinct and the front appears rough and wrinkled rather than smooth. Isolated, small-scale (less than 1 mm in width), regions of low fluorescence are observed within the high intensity region behind the main reaction front. Close inspection of these wrinkled fronts suggests that significant fluctuations in temperature, concentration and velocity are occurring at the submillimeter scale, approximately two orders of magnitude lower than that of the dominant cell width.

Manzhalei [28] proposed a minimum activation energy criterion of $E_a/RT_{vN} \geq 6.5$ for substructure to occur. Manzhalei's criterion is satisfied by the hydrocarbon mixtures in this study while some N_2-diluted H_2 mixtures exceed this activation energy by up to 30% and do not have substructure. The presence of substructure on soot foils in these mixtures indicates that the corrugated appearance of these fronts is at least partially due to the superposition of cellular structure occurring over a range of scales.

The variation in the range of scales with activation energy appears to be a straight forward consequence of the Arrhenius dependence of the reaction rates and the lead shock velocity oscillation. We have estimated [9] the induction zone length as a function of the lead shock strength (Fig. 7) for three representative cases using a detailed chemical kinetics mechanism [30]. It is clear that the higher the activation energy, the larger the range of scales for a given range of shock velocity oscillation amplitudes. Both the range of reaction zones lengths and the transverse wave spacings (cell width) shown in Fig. 7 for unstable mixtures are consistent with this explanation. In addition, the highly unstable mixtures apparently have a larger [31] amplitude oscillation than the weakly unstable cases [21]. The very long induction times predicted for low shock velocities, $U \sim 0.8U_{CJ}$, may lead to local decoupling of the lead shock and reaction near the end of the cell. We investigated this possibility by applying the critical decay rate model of Eckett et al. [21] to the numerical data of Gamezo et al. [31]. We find that in the case of θ=7.4, local decoupling of the detonation occurs at the end of the cell cycle [9].

A possible case of decoupling is observed in a high-speed shadowgraph movie made using a rotating mirror camera. In highly unstable fronts, a local explosion is observed to occur during a transverse wave interaction, Fig. 8. This explosive interaction contrasts substantially with the less dramatic interaction observed in the weakly unstable mixtures. A "microexplosion" at the cell apex was also observed by Vasiliev and Nikolaev [32] in C_2H_2-2.5O_2, P_1=1.0 kPa in a 5×60 mm channel.

7. Conclusions

Mixtures with higher activation energy have markedly different structure than those with low activation energy. Two effects are apparent when the activation energy is increased: a greater number of unstable modes are present resulting in superposition of structure over a broad range of scales, and the magnitude of the lead shock oscillation through a cell cycle increases, possibly resulting in local decoupling during the low-amplitude portion of the oscillation cycle.

The distortions of the OH and shock fronts over a wide range of scales (a factor of at least 100 and possibly as high as 1000) immediately suggests that this may be a type of "turbulent" combustion. However, although the reaction and shock fronts are highly distorted, simple estimates of reaction zone length indicate that in large measure the distortions may be attributed to the usual detonation chemical-hydrodynamic instability and that the combustion may in fact still be proceeding by the usual diffusionless [33] branching chain-thermal explosion mechanism.

On the other hand, our PLIF images clearly indicate that there are significant flucutations in OH concentration within the reaction zone. Evidence of shear layers and associated velocity fluctuations have also been observed in both schlieren and OH PLIF images. These fluctuations may be evidence of turbulent mixing that ultimately leads to molecular mixing and enhancements in the reaction rate over the diffusionless values. At this time, the issue is still open. The extent to which mixing and diffusion play a role in these highly unstable detonations is the subject of ongoing [33] and future investigation with a substantial role for both improved experimental techniques, analysis, and numerical simulation.

Acknowledgments

This work was supported in part by funding from the ONR and the Caltech ASCI ASAP Center for Simulation of the Dynamic Response of Materials.

References

[1] B. V. Voitsekhovskii, V. V. Mitrofanov, and M. E. Topchian. Struktura fronta detonastii i gaza. *Akad. Nauk., SSSR, Novosibirsk*, 1963. Translation: The structure of a detonation front in gases Rep. FTD-MT-64-527, Foreign Technology Division, Wright-Patterson A.F.B., Ohio,(1966).

[2] R. A. Strehlow. *Phys. Fluids*, 7:908–9, 1964.

[3] A.K. Oppenheim, J.J. Smolen, and L.J. Zajac. *Combust. Flame*, 12:63–76, 1968.

[4] P. A. Urtiew. *Astronautica Acta*, 15:335–343, 1970.

[5] D. H. Edwards, G. Hooper, and R. J. Meddins. *Astronautica Acta*, 17(4-5):475–485, 1972.

[6] Florian Pintgen. *Laser-Optical Visualization of Detonation Structures*. Diplom Arbeit, Lehrstuhl für Thermodynamik: Technische Universität München / Graduate Aeronautical Laboratories: California Institute of Technology, December 2000.

[7] F. Pintgen, J. M. Austin, and J. E. Shepherd. In G.D. Roy, S.M. Frolov, R.J. Santoro, and S.A. Tsyganov, editors, *Confined Detonations and Pulse Detonation Engines*, pages 105–116. Torus Press, Moscow, 2003.

[8] F. Pintgen, C. A. Eckett, J. M. Austin, and J. E. Shepherd. *Combust. Flame*, 133(3):211–229, 2003.
[9] Joanna Austin. *The Role of Instability in Gaseous Detonation*. PhD thesis, California Institute of Technology, Pasadena, California, June 2003.
[10] I. O. Moen, J. W. Funk, S. A. Ward, G. M. Rude, and P. A. Thibault. *Prog. Aeronaut. Astronaut.*, 94:55–79, 1984.
[11] I. O. Moen, A. Sulmistras, G. O. Thomas, D. Bjerketvedt, and P. A. Thibault. *Prog. Astronaut. Aeronaut.*, 106:220–243, 1986.
[12] D. Desbordes. *Prog. Astronaut. Aeronaut.*, 114:170–185, 1988.
[13] M. I. Radulescu and J. H. S Lee. *Combust. Flame*, 131 (1-2):29–46, 2002.
[14] R.A. Strehlow. *Astronautica Acta*, 14:539–548, 1969.
[15] J. C. Libouton, A. Jacques, and P. J. Van Tiggelen. Cinétique, structure et entretien des ondes de détonation. *Actes du Colloque International Berthelot-Vieille-Mallard-Le Chatelier*, 2:437–442, 1981. Bordeaux.
[16] J. E. Shepherd, I. O. Moen, S. B. Murray, and P. A. Thibault. Analysis of the cellular structure of detonations. *21st Symp. (Int.) Combust.*, pages 1649–1657, 1986.
[17] V. Yu. Ul'yanitskii. *Fizika Goreniya i Vzryva*, 17:227, 1981.
[18] H. I. Lee and D. S. Stewart. *J. Fluid Mech.*, 216:103–132, 1990.
[19] J. J. Erpenbeck. *Phys. Fluids*, 7:684–696, 1964.
[20] M. Short and D. S. Stewart. *J. Fluid Mech.*, 368:229–262, 1998.
[21] Christopher A. Eckett. *Numerical and Analytical Studies of the Dynamics of Gaseous Detonations*. PhD thesis, California Institute of Technology, Pasadena, California, September 2000.
[22] W. C. Reynolds. The element potential for chemical equilibrium analysis: implementation in the interactive program STANJAN. Technical Report A-3991, Dept. of Mechanical Engineering, Stanford University, Stanford, CA, January 1986.
[23] E. Schultz and J. E. Shepherd. Validation of detailed reaction mechanisms for detonation simulation. Technical Report FM99-5, Graduate Aeronautical Laboratories: California Institute of Technology, 2000.
[24] R.A. Strehlow and A.J. Crooker. *Acta Astronautica*, 1: 303–315, 1974.
[25] S. I. Jackson and J. E. Shepherd. Technical Report AIAA 2002-3627, 38th AIAA/ASME/SAE/ASEE Joint Propulsion Conference, Indianapolis, IN, July 7-10 2002.
[26] Raza Akbar. *Mach Reflection of Gaseous Detonations*. PhD thesis, Rensselaer Polytechnic Institute, Troy, New York, August 1997.
[27] Eric Schultz. *Detonation Diffraction Through an Abrupt Area Expansion*. PhD thesis, California Institute of Technology, Pasadena, California, April 2000.
[28] V. I. Manzhalei. *Fizika Goreniya i Vzryva*, 13(3):470–472, 1977.
[29] V. Gamezo, A.M.Khokhlov, E.S.Oran, Secondary detonation cells in systems with high activation energy *Proc. of the 17th ICDERS*, Heidelberg, 1999.
[30] A.A. Konnov. *http://homepages.vub.ac.be/ akonnov*, 1998.
[31] V. N. Gamezo, D. Desbordes, and E. S. Oran. *Shock Waves*, 9:11–17, 1999.
[32] A. A. Vasiliev and Yu. Nikolaev. *Acta Astronaut.*, 5: 983–996, 1978.
[33] S. Singh, D. Lieberman, and J. E. Shepherd. Combustion behind shock waves. Paper 03F-29 Western States Section/Combustion Institute, October 2003.
[34] J. E. Shepherd. *Prog. Astronaut. Aeronaut.*, 106:263–293, 1986.
[35] J. Warnatz and V. Karbach. *http://www.ca.sandia.gov /tdf/3rdWorkshop/ch4mech.html*, 1997.
[36] M. A. Mueller, R. A. Yetter, and F. L. Dryer. *Int. J. Chem. Kinetics*, 32(6):317–339, 2000.
[37] Philip A. Thompson. *Compressible–Fluid Dynamics*. Rensselaer Polytechnic Institute, 1988.

Table 1: Some calculated detonation front mixture parameters. The induction length Δ is calculated using the ZND code [34] and a detailed chemical kinetics mechanism. The normalized activation energy θ is calculated as described in the text. The Warnatz and Karbach [35] mechanism was used for ethylene mixtures, the Mueller et al. [36] mechanism for N_2O mixtures and the Konnov [30] mechanism for all others. The normalized chemical energy release Q is calculated from the CJ Mach number assuming a two-gamma model [37]. U_{CJ}, γ_1, γ_2, T_{vN}, and P_{vN} are calculated using STANJAN. T_{vN}, and P_{vN} are the temperature and pressure at the post-shock (von Neumann) state. Parameters are calculated at 20 kPa initial pressure, and 298 K nominal initial temperature.

Mixture	U_{CJ} (m/s)	Δ (mm)	γ_1	γ_2	T_{vN} (K)	P_{vN} (MPa)	θ	Q	Instability
$2H_2$-O_2-12Ar	1517.9	0.7	1.602	1.288	1899.3	0.41	5.2	24.2	weak
$2H_2$-O_2-17Ar	1415.0	1.3	1.622	1.397	1775.3	0.44	5.4	14.7	weak
$2H_2$-O_2-3.5N_2	1958.0	0.7	1.390	1.163	1501.4	0.54	6.2	45.3	moderate
$2H_2$-O_2-5.6N_2	1796.6	1.4	1.405	1.185	1403.2	0.49	6.9	36.3	moderate
H_2-N_2O-1.33N_2	2017.5	1.5	1.342	1.170	1613.7	0.72	11.1	55.2	high
H_2-N_2O-1.77N_2	1954.7	2.3	1.346	1.171	1574.4	0.68	11.5	52.2	high
C_2H_4-3O_2-8N_2	1870.1	2.6	1.271	1.161	1627.4	0.72	12.4	53.7	high
C_2H_4-3O_2-10.5N_2	1844.1	3.2	1.370	1.161	1613.5	0.69	12.1	56.9	high
C_3H_8-5O_2-9N_2	1934.4	1.7	1.336	1.161	1643.7	0.82	12.7	65.3	high

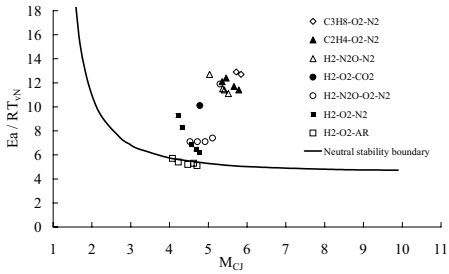

Fig. 1: Categorization of detonation front structure from stability considerations. Parameters [9] for mixtures considered in this study (symbols) are compared to the neutral stability boundary from Lee and Stewart [18].

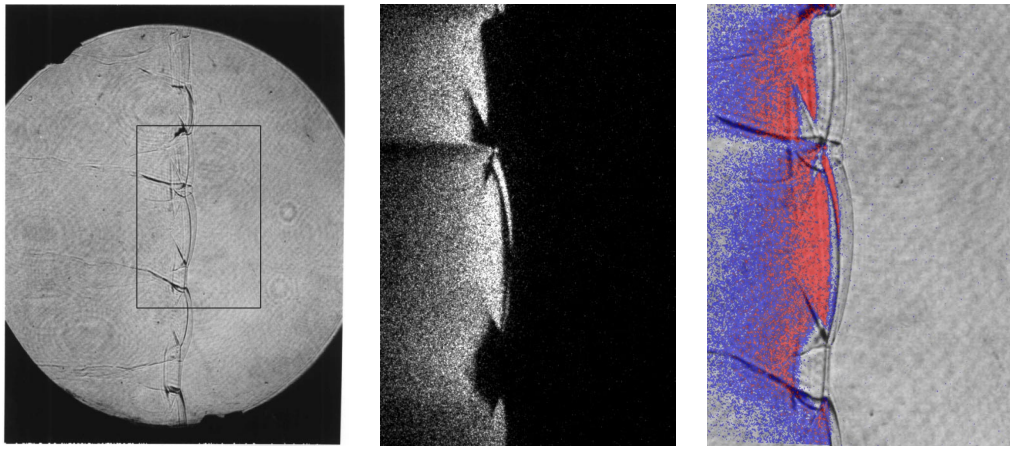

(a) (b) (c)

Fig. 2: Images of detonation front propagating from left to right in $2H_2$-O_2-12Ar, P_1=20 kPa in the narrow channel. (a) Schlieren image. The box shows the location of the corresponding OH fluorescence image shown in (b). (c) Superimposed schlieren and fluorescence image (the false color is a function of the intensity of the signal). PLIF image is 60 mm high.

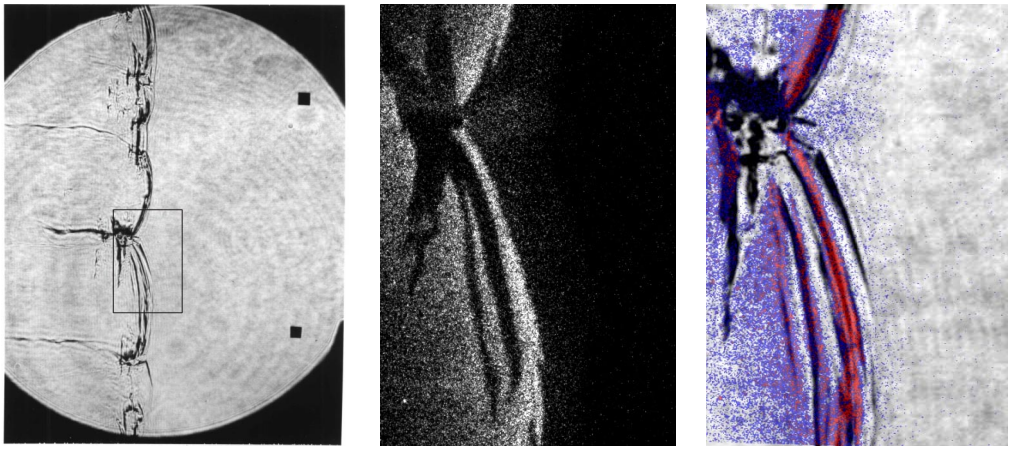

(a) (b) (c)

Fig. 3: Images of detonation front propagating from left to right in $2H_2$-O_2-$3.5N_2$, P_1=20 kPa in the narrow channel. (a) Schlieren image. The box shows the location of the corresponding OH fluorescence image shown in (b). (c) Superimposed schlieren and fluorescence images. PLIF image is 30 mm high.

Fig. 4: PLIF images of detonation front propagating from left to right in $2H_2$-O_2-$4.5N_2$, P_1=20 kPa in the narrow channel. Image is 30 mm high.

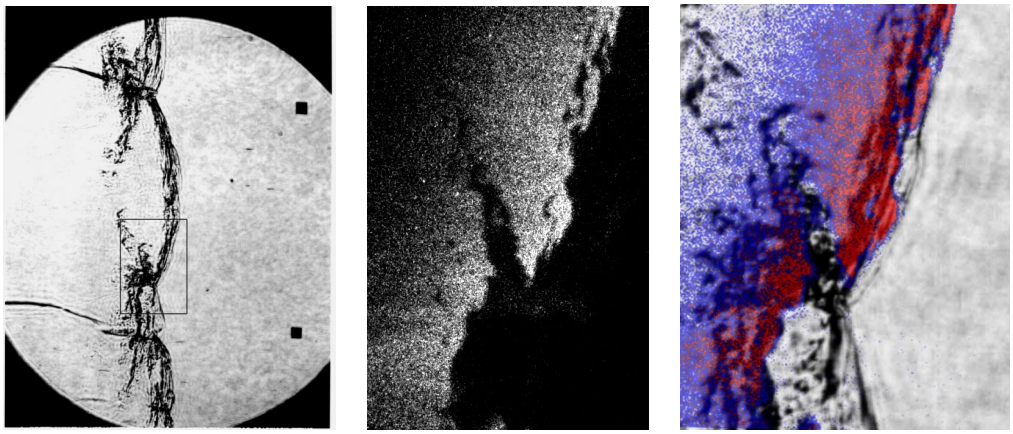

(a) (b) (c)

Fig. 5: Images of a detonation front propagating from left to right in C_2H_4-$3O_2$-$10.5N_2$, P_1=20 kPa in the narrow channel. (a) Schlieren image. The box shows the location of the corresponding OH fluorescence image shown in (b). (c) Superimposed schlieren and fluorescence image. PLIF image is 30 mm high.

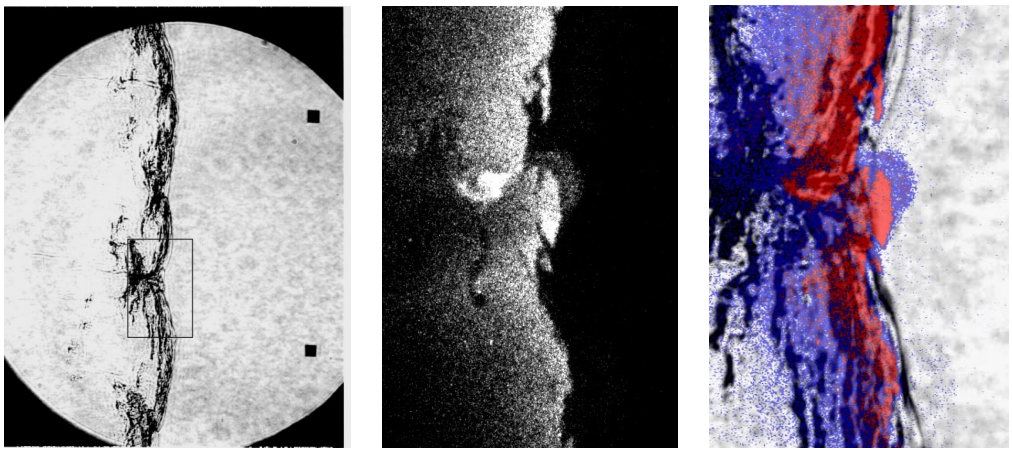

(a) (b) (c)

Fig. 6: Images of a detonation front propagating from left to right in C_2H_4-$3O_2$-$8N_2$, P_1=20 kPa in the narrow channel. (a) Schlieren image. The box shows the location of the corresponding OH fluorescence image shown in (b). (c) Superimposed schlieren and fluorescence image. PLIF image is 30 mm high.

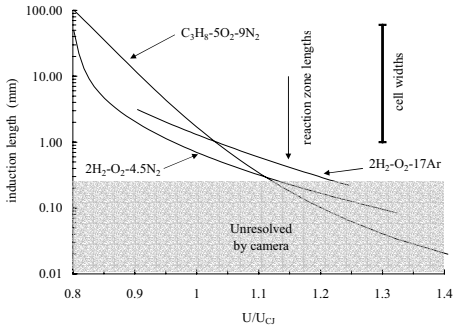

Fig. 7: Calculated reaction zone lengths as a function of normalized lead shock velocity for three representative cases. The range of cell sizes and observable reaction zone length fluctuations for unstable mixtures is also shown together with the estimated resolution limits of the PLIF camera.

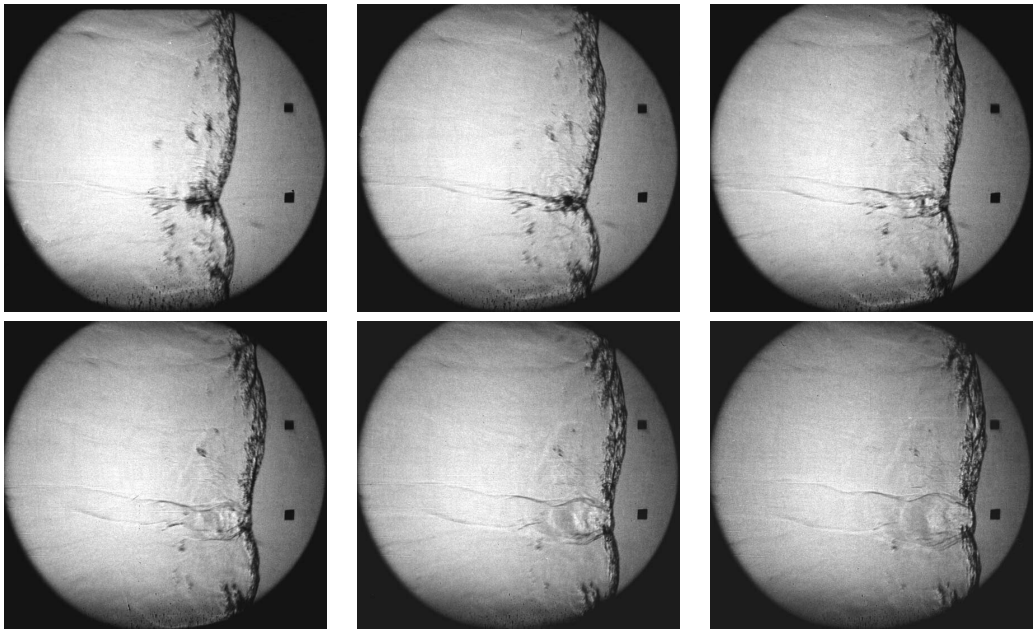

Fig. 8: Time-resolved shadowgraph images of a detonation propagating in C_3H_8-$5O_2$-$9N_2$ in the narrow channel. Time between frames is 1.6 μs. Field of view is about 138 mm.